ISSN 1674-1056
http://cpb.iphy.ac.cn
http://iopscience.iop.org/cpb
中国物理 B
Chinese Physics
中国物理 Chinese Physics B

Fine structures of defect cores induced by elastic anisotropy and biaxiality in hybrid alignment nematics

Xuan Zhou(周璇), Si-Bo Chen(陈思博), Zhi-Dong Zhang(张志东)
Citation: Chin. Phys. B . 2018, 27(5): 056103. **doi:** 10.1088/1674-1056/27/5/056103

Journal homepage: http://cpb.iphy.ac.cn; http://iopscience.iop.org/cpb

What follows is a list of articles you may be interested in

Theoretical analysis of the influence of flexoelectric effect on the defect site in nematic inversion walls

Gui-Li Zheng(郑桂丽), Hui Zhang(张辉), Wen-Jiang Ye(叶文江),Zhi-Dong Zhang(张志东), Hong-Wei Song(宋宏伟), Li Xuan(宣丽)
Chin. Phys. B . 2016, 25(3): 036101. **doi:** 10.1088/1674-1056/25/3/036101

Dynamics of a ± 1/2 defect pair in a confined geometry: A thin hybrid aligned nematic cell

Lu Li-Xia, Zhang Zhi-Dong
Chin. Phys. B . 2015, 24(2): 026102. **doi:** 10.1088/1674-1056/24/2/026102

Phase behaviors of binary mixtures composed of banana-shaped and calamitic mesogens

M. Cvetinov, D. Ž. Obadović, M. Stojanović, A. Vajda, K. Fodor-Csorba, N. Eber, I. Ristić
Chin. Phys. B . 2014, 23(9): 096402. **doi:** 10.1088/1674-1056/23/9/096402

Fine structures of defect cores induced by elastic anisotropy and biaxiality in hybrid alignment nematics*

Xuan Zhou(周璇)[1], Si-Bo Chen(陈思博)[2,3], and Zhi-Dong Zhang(张志东)[1,†]

[1] *Department of physics, Hebei University of Technology, Tianjin* 300401, *China*
[2] *School of Electronic and Information Engineering, Hebei University of Technology, Tianjin* 300401, *China*
[3] *Tianjin Key Laboratory of Electronic Materials and Devices, Tianjin* 300401, *China*

(Received 7 February 2018; revised manuscript received 9 March 2018; published online 26 April 2018)

Based on Landau–de Gennes theory and two-dimensional finite-difference iterative method, the spontaneous distortion in hybrid alignment nematic cells with $M = \pm 1/2$ disclination lines is investigated by establishing two models. The fine structures of defect cores are described in the order space S^2/Z_2. The joint action of elastic anisotropy (L_2/L_1) and biaxiality of defects induces the spontaneous twist distortion, accompanied by the movement of the defect center to the upper or lower plate. For each model, four mixed defect structures appear with the same energy, which are defined as energetically degenerated quadruple states.

Keywords: Landau–de Gennes theory, elastic anisotropy, mixed defects, order space

PACS: 61.30.JF, 64.70.M– **DOI:** 10.1088/1674-1056/27/5/056103

1. Introduction

Topological defects, found in systems with broken continuous symmetry, are ubiquitous in nature, from microscopic condensed matter systems governed by quantum mechanics to a universe in which gravity plays a decisive role.[1–3] Defects in liquid crystals (LCs) have been the subject of much interest, still offering unsolved problems. A topological charge M of integer or half-integer can be assigned to each defect. One value of topological charge $M = \pm 1/2$ characterizes the entire class of stable defects in nematics.[1] All other half-integer-valued lines, whether positive or negative, can be continuously deformed into a line with charge $\pm 1/2$ and integer-valued lines can "escape in the third dimension".[4]

Topological defects can also be classified by homotopy groups.[5–7] In a three-dimensional (3D) nematic liquid crystal (NLC) system, due to the equivalence between the head and the tail of the director (or that $\boldsymbol{n}$ and $-\boldsymbol{n}$), the order space is S^2/Z_2 (where S^2 is a homotopy group of the sphere, and Z_2 is the Abelian group with two elements). Each defect can be represented by a contour in S^2/Z_2. The director $\boldsymbol{n}$ rotates by an angle of $2\pi M$ along the contour encircling the defect. Contours of defects with integer charge are actually closed (e.g., circles) and can shrink into a point, indicating that the defects are topologically unstable.[8] While the contours of defects with half-integer charge terminate at two diametrically opposite points; under any continuous deformations, the ends of these contours remain fixed at the diametrically opposite points, indicating that the defects are topologically stable.[5]

A defect line parallel to the rotation axis of $\boldsymbol{n}$ is referred to as wedge disclination; while a defect line perpendicular to the rotation axis of $\boldsymbol{n}$ is referred to as twist disclination.[5] Note that the intermediate case where the defect line neither parallel nor perpendicular to the rotation axis of $\boldsymbol{n}$ is possible, which we refer to as mixed disclination.[9–12] Fukuda *et al.*[6] have realized the transformation of a $-1/2$ wedge disclination line to a $+1/2$ one in a numerical simulation, and mixed disclinations appeared during the transformation.

The region where the presence of a defect causes the apparent deviation from bulk ordering is referred to as defect core, which is difficult to explore experimentally, as their spatial extension is very small, usually a few molecular lengths, which makes it practically impossible to use standard optical or electron microscopy in studying the properties of the core.[13,14] Because of very limited experimental data, modern theories of the topological defects treat the core problem under a number of strong simplified assumptions,[15–17] such as the one-elastic-constant approximation ($K_{11} = K_{22} = K_{33} = K$), the director $\boldsymbol{n}$ is confined in a two-dimensional (2D) plane. Zhou *et al.*[18] explored the cores of disclinations in the chromonic nematics that extend over macroscopic length scales accessible for optical characterization, but they did not give the precise director profile around the core. So far the fine structure of the core region of defects is also one of the most difficult problems, especially on condition that the director is not confined in a 2D plane, which has gained increasing research attention.

In this study, we investigate the structural transition in a hybrid alignment nematic (HAN) layer with $M = \pm 1/2$ topo-

*Project supported by the National Natural Science Foundation of China (Grant Nos. 11374087 and 11447179) and the Key Subject Construction Project of Hebei Province University, China.

†Corresponding author. E-mail: zhidong_zhang1961@163.com

© 2018 Chinese Physical Society and IOP Publishing Ltd

logical defect theoretically. Our study is based on the Landau–de Gennes theory describing the orientational order of an LC in terms of a second-rank tensor Q, which encompasses both uniaxial and biaxial states.[19] Mixed defect structures induced by elastic anisotropy are found and the fine structures of defect core are given. The rest of this paper is organized as follows. In Section 2, we introduce the phenomenological model to be employed here in this paper and describe the geometry of the problem and our parameterization. The results are presented in Section 3, and the conclusions are drawn from the present studies in Section 4.

2. Theoretical basis

2.1. Free energy

Our theoretical argument is based on Landau–de Gennes theory,[19] in which the orientational order of LC is described by a second-rank symmetric and traceless tensor[20]

$$Q=\sum_{i=1}^{3}\lambda_i \boldsymbol{e}_i\otimes\boldsymbol{e}_i. \tag{1}$$

Here, $\boldsymbol{e}_i$ is the orthogonal unit vector representing the eigenvector of Q, and λ_i is its eigenvalue. The range of eigenvalues must be $\lambda_i\in(-1/3,2/3)$ to explain Q as a traceless second-moment tensor of the molecular distribution function. In the isotropic phase Q vanishes, whereas this parameter has two degenerate eigenvalues in the uniaxial ordering and can be represented by

$$Q=S\left(\boldsymbol{n}\otimes\boldsymbol{n}-\frac{1}{3}\boldsymbol{I}\right), \tag{2}$$

where $\boldsymbol{n}$ is the nematic director pointing along the local uniaxial ordering direction, and S is the uniaxial scalar parameter expressing the magnitude of fluctuations about the nematic director. In Eq. (2), S can be either positive or negative. The ensemble of molecules represented by Q tends to align along $\boldsymbol{n}$ when S is positive and tends to lie in the plane orthogonal to $\boldsymbol{n}$ when S is negative. Finally, the LC is in a biaxial state when all the eigenvalues of Q are different from each other. The degree of biaxiality is expressed by the parameter β^2 defined as[21]

$$\beta^2=1-\frac{6\left[\mathrm{tr}\left(Q^3\right)\right]^2}{\left[\mathrm{tr}\left(Q^2\right)\right]^3}. \tag{3}$$

This equation is of a convenient parameter for illustrating spatial inhomogeneities of Q, and the value of β^2 is in a range of [0, 1]. All uniaxial states with two degenerate eigenvalues correspond to $\beta^2=0$, whereas states with maximal biaxiality correspond to $\beta^2=1$. As $\mathrm{tr}(Q^3)=3\det Q$, states with $\beta^2=1$ are those with $\det Q=0$, which implies that at least one eigenvalue of Q vanishes. As is well known, the regions of defect cores are biaxially textured.[15–17]

The Landau–de Gennes free energy density of LC is given by $f=f_{\mathrm{bulk}}\{Q_{\alpha\beta}\}+f_{\mathrm{e}}\{Q_{\alpha\beta},\nabla\}$, in which

$$f_{\mathrm{bulk}}=\frac{A}{2}\mathrm{tr}Q^2-\frac{B}{3}\mathrm{tr}Q^3+\frac{C}{4}\left(\mathrm{tr}Q^2\right) \tag{4}$$

is the bulk energy that describes a homogeneous phase. In f_{bulk}, B and C are positive constants, and A is assumed to vary with temperature T in the form $A=a(T-T^*)$, where a is a positive constant and T^* is the nematic supercooling temperature. Equation (4) gives the bulk equilibrium value of the uniaxial scalar order parameter in Eq. (2),

$$S=\frac{B}{4C}\left(1\pm\sqrt{1-\frac{24AC}{B^2}}\right),$$

which also depends on temperature.

The free energy, f_{e}, which penalizes gradients in the tensor order parameter field, is given by

$$F_{\mathrm{e}}=\frac{1}{2}L_1\left(\frac{\partial Q_{ij}}{\partial x_k}\frac{\partial Q_{ij}}{\partial x_k}\right)+\frac{1}{2}L_2\left(\frac{\partial Q_{ij}}{\partial x_j}\frac{\partial Q_{ik}}{\partial x_k}\right), \tag{5}$$

where L_1 and L_2 are elastic constants. According to the Frank theory, we obtain the relationship between L_i and K_{ii} as

$$L_1=\frac{K_{22}}{2S^2},\quad L_2=\frac{K_{11}-K_{22}}{S^2}.$$

Here, we assume $K_{11}=K_{33}\neq K_{22}$ just for simplicity.

2.2. Models and geometry of the problem

We choose a HAN cell in strong anchoring boundary conditions, and the nematic director is parallel to one wall and perpendicular to the other (see Fig. 1). The plates are placed at $z=\pm d/2$ of a Cartesian coordinate system. The lengths, d_x and d_y, of the cell along the x- and the y-axes are much larger than d ($d_x\sim d_y\gg d$).

We study HAN structures with $M=-1/2$ wedge disclination (Model I), and $M=+1/2$ wedge disclination (Model II). The disclination line is parallel to the y-axis of the simulation cells, and we seek solutions independent of y.

To describe the configuration, the nematic director is given by

$$\boldsymbol{n}=\sin\theta\cos\varphi\boldsymbol{e}_x+\sin\theta\sin\varphi\boldsymbol{e}_y+\cos\theta\boldsymbol{e}_z,$$

where θ is the polar angle between the z-axis and the director $\boldsymbol{n}$, and φ is the twist angle between the x-axis and the x–y projection of the director. In the coordinate system, Q can be written as

$$Q=S\begin{pmatrix}\sin^2\theta\cos^2\varphi-\frac{1}{3} & \sin^2\theta\sin\varphi\cos\varphi & \sin\theta\cos\theta\cos\varphi\\ \sin^2\theta\sin\varphi\cos\varphi & \sin^2\theta\sin^2\varphi-\frac{1}{3} & \sin\theta\cos\theta\sin\varphi\\ \sin\theta\cos\theta\cos\varphi & \sin\theta\cos\theta\sin\varphi & \cos^2\theta-\frac{1}{3}\end{pmatrix}. \tag{6}$$

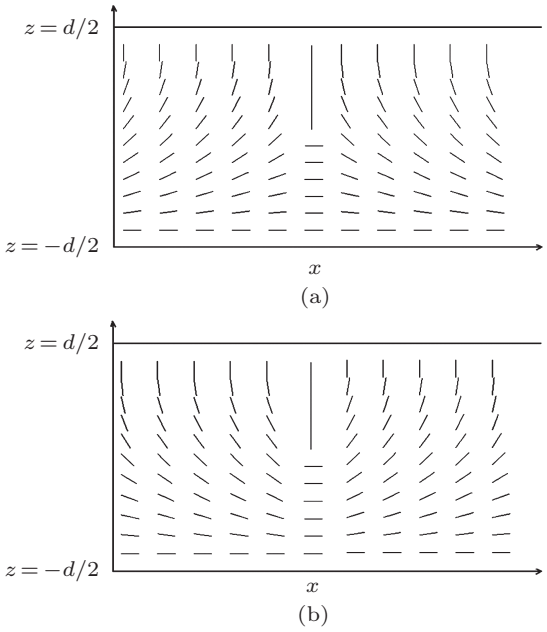


Fig. 1. Geometries of (a) Model I and (b) Model II.

At $z = \pm d/2$, we enforce the uniaxial strong anchoring represented by $\theta_{-d/2} = \pi/2$, $\varphi_{-d/2} = 0$ and $\theta_{+d/2} = 0$, $\varphi_{+d/2} = 0$, that is

$$Q_{-d/2} = S\begin{pmatrix} \frac{2}{3} & 0 & 0 \\ 0 & -\frac{1}{3} & 0 \\ 0 & 0 & -\frac{1}{3} \end{pmatrix}, \quad Q_{+d/2} = S\begin{pmatrix} -\frac{1}{3} & 0 & 0 \\ 0 & -\frac{1}{3} & 0 \\ 0 & 0 & \frac{2}{3} \end{pmatrix}.$$

On the lateral walls at $x = \pm d_x/2$, we denote the free boundary conditions with initial uniaxial ordering. For Model I, the total rotation at $x = +d_x/2$ is $-\pi/2$, while at $x = -d_x/2$ it is $\pi/2$. We obtain Model II by exchanging the lateral walls (see Fig. 1).

2.3. Scaling and dimensionless evolution equations

We introduce the following dimensionless quantities:

$$\tilde{f} \equiv f \Big/ \left[\frac{B^4}{(4C)^3}\right], \quad \tilde{Q}_{ij} \equiv Q_{ij}/q_0, \quad \tilde{z} \equiv z/\xi_0, \quad \tilde{x} \equiv \tilde{x}/\xi_0,$$

where $q_0 = B/4C$ is the superheating order parameter at the nematic superheating temperature T^{**}, and

$$\xi_0 = \sqrt{\frac{L}{Bq_0}} = \sqrt{\frac{4CL}{B^2}}$$

is the characteristic length for order parameter changes. Equations (4) and (5) can be reduced respectively to

$$\tilde{f}_{\text{bulk}} = \frac{\tilde{A}}{12}\text{tr}\tilde{Q}^2 - \frac{1}{3}\text{tr}\tilde{Q}^3 + \frac{1}{16}\left(\text{tr}\tilde{Q}^2\right)^2, \tag{7}$$

$$\tilde{f}_{\text{elastic}} = \frac{1}{2}\left(\frac{\partial \tilde{Q}_{ij}}{\partial \tilde{x}_k}\frac{\partial \tilde{Q}_{ij}}{\partial \tilde{x}_k}\right) + \frac{1}{2}\frac{L_2}{L_1}\left(\frac{\partial \tilde{Q}_{ij}}{\partial \tilde{x}_j}\frac{\partial \tilde{Q}_{ik}}{\partial \tilde{x}_k}\right), \tag{8}$$

where the reduced parameter $\tilde{A} = 24AC/B^2$ is defined as the temperature scale. The isotropic-nematic transition occurs at $\tilde{A} = 8/9$. Thus, the reduced uniaxial ordering has the form

$$\tilde{Q} = \tilde{S}\left(\boldsymbol{n}\otimes\boldsymbol{n} - \frac{1}{3}I\right), \tag{9}$$

where $\tilde{S} = S_{\text{eq}}/q_0 = 1 + \sqrt{1-\tilde{A}}$ is the reduced uniaxial scalar parameter in equilibrium.

We compute the evolution of LC with a dynamic theory for tensor order-parameter field $Q(r, t)$. The local values of the scalar order parameter S and the director $\boldsymbol{n}$ can be calculated from Q by using the highest eigenvalue and the associated eigenvector, respectively. According to Ref. [22], the evolution equation describing the dynamics of Q can be written as

$$\frac{\partial Q}{\partial t} = \Gamma\left[-\frac{\delta f}{\delta Q} + \frac{1}{3}\text{tr}\left(\frac{\delta f}{\delta Q}\right)I\right], \tag{10}$$

where $\Gamma = 6D^*/[1-3\text{tr}(Q^2)]^2$, with D^* being the rotational diffusion for the nematic; $\delta f/\delta Q$ is assumed to be symmetrical.

Numerical calculations are performed using the reduced variables. When the functional derivatives in Eq. (10) are evaluated, the following evolution equations for $\tilde{Q}$ can be obtained:

$$\begin{aligned}\frac{\partial \tilde{Q}}{\partial t} = &-\tilde{\Gamma}\left[\frac{A}{6}\tilde{Q} - \tilde{Q}^2 + \text{tr}\left(\tilde{Q}^2\right)\left(\frac{\tilde{Q}}{4} + \frac{1}{3}I\right) - \tilde{\nabla}^2\tilde{Q}\right. \\ &\left. - \frac{L_2}{L_1}\left(\tilde{\nabla}\cdot\tilde{Q}\right)\cdot\left(\tilde{\nabla}\cdot\tilde{Q}\right)\right],\end{aligned} \tag{11}$$

with $\tilde{\Gamma} = \Gamma \times (Bq_0)$. The value of L_2/L_1 represents the magnitude of the elastic anisotropy. A larger value of L_2/L_1 corresponds to a smaller twist elastic constant K_{22}.

We adopt the two-dimensional finite-difference method developed in our previous studies to obtain the numerical simulation results.[23–25] Here, the system is relaxed from an initial boundary condition given in Subsection 2.2, and the initial conditions of the left half and right half in the bulk are consistent with the boundary conditions at the left wall and right wall given above. The initial perturbation of twist angle is given as follows: from $z = -d/2$ to $z = d/2$, the twist angle changes as $\pi/2 \times \sin[\pi \times (z + d/2)/d]$ or $-\pi/2 \times \sin[\pi \times (z + d/2)/d]$. That means that the initial twist angle is zero on the lower and upper plates, and $\pm\pi/2$ in the middle of the nematic cell. For each model, there are four forms of the initial perturbations distinguished by the signs of the initial twist angle on the left and right half. For example, if the initial twist angles are both positive on the left and right half in the bulk, we express it as +(left) +(right) (Form A); similarly, we can write other three forms as −(left)−(right) (Form B), +(left)−(right) (Form C), and −(left)+(right) (Form D).

We consider only the equilibrium configurations that correspond to the global minimum F. In our numerical calculations, a discretization in time steps of 10^{-8} s is sufficient to guarantee the stability of the numerical procedure. In addition, our equilibration runs take 2×10^6 steps in total which is adequate for the system to reach the equilibrium.

3. Results

According to parameters given in Ref. [26], $a = 0.195\times10^6$ J/m^3, $B = 7.155\times10^6$ J/m^3, $C = 8.82\times10^6$ J/m^3, $L_1 = 10.125\times10^{-12}$ J/m can be easily obtained. In our simulations, the scaled temperature is set to be $\tilde{A} = 2/3$, which corresponds to $\tilde{s} = 1+\sqrt{1/3}$. The rotational diffusion D^* is set to be 0.35, which is the value used in Ref. [26]. The cell gap is set to be $d = 300\xi_0$. We then obtain the exact value $\xi_0 = 2.64$ nm and the cell gap $d = 300\xi_0 \approx 0.8$ μm. The elastic anisotropy is set to be $L_2/L_1 = 5$, corresponding to $K_{22}/K_{11} = 2/7$. We focus on the dependence of structure transition on elastic anisotropy.

In order to present the results in the order space S^2/Z_2, we introduce Θ and Φ to redefine the director $\boldsymbol{n}$ at equilibrium state, where $\Theta\in[0,\pi/2]$ is the angle between the director $\boldsymbol{n}$ and the x–z plane, to show the deviation of the director from the x–z plane induced by elastic anisotropy L_2/L_1, and $\Phi\in[-\pi,\pi]$ is the angle between the x-axis and the x–z projection of the director (see Fig. 2). Here, all directors are redefined into an upper hemisphere representing the order space S^2/Z_2, according to the y-component of the director, n_y. If $n_y\geq0$, the director $\boldsymbol{n}$ maintains to be in the upper hemisphere; while if $n_y<0$, $\boldsymbol{n}$ changes into $-\boldsymbol{n}$ to ensure it in the upper hemisphere.

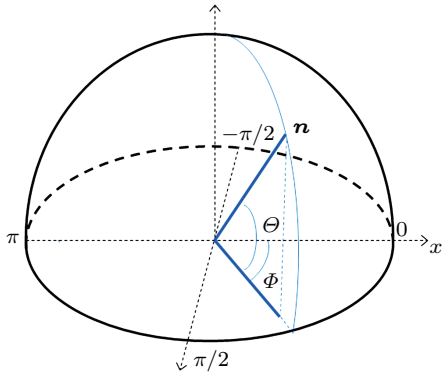


Fig. 2. (color online) Order space S^2/Z_2 for the nematic phase.

3.1. Structure transition of Model I

3.1.1. Structures of Forms A and B

Figure 3 shows the profiles of Θ and Φ of the director at equilibrium state for the case of Form A. It is seen clearly that the defect center moves to the upper plate. In addition, the elastic anisotropy induces the spontaneous distortion, and the maximum distortion exists near the defect center (see Fig. 3(a)). For further explanation of the spontaneous distortion, we give the y-component of the director, n_y, in Fig. 4, and the figure also shows that the maximum distortion exists around the defect center. Along the contour that we plotted, the new structure can be explained in the order space S^2/Z_2 by Fig. 7(a). The point o on the contour is the starting point, and is also the terminal point o' of the contour. This point corresponds to two diametrically opposite points on the bottom circle of the hemisphere in Fig. 7(a). The value of Θ changes from 0 to a maximum value $\Theta_{\max}$ between 0 and $\pi/2[\Theta_{\max}\in(0,\pi/2)]$, and then turns back to 0; meanwhile, Φ changes from $\pi/2$ to 0 and then to $-\pi/2$. Here we should notice that the value of $\Theta_{\max}$ depends on the contour that we plotted. It is seen clearly in Fig. 7(a) that the rotation axis of $\boldsymbol{n}$ is neither parallel nor perpendicular to the defect line (y-axis), thus the new defect structure is a mixed disclination.

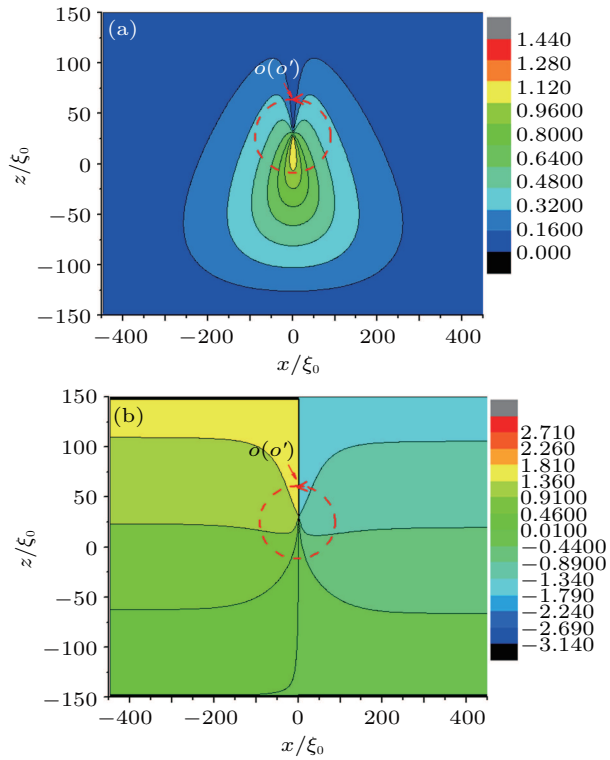


Fig. 3. (color online) Profiles of configurations (a) Θ and (b) Φ of director at equilibrium state for Form A of Model I.

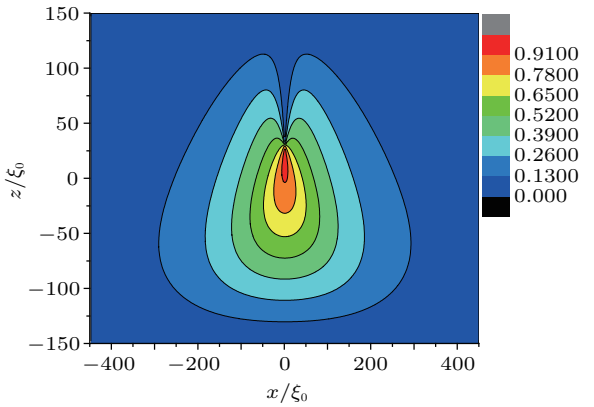


Fig. 4. (color online) Profile of n_y component of director at equilibrium state for Form A of Model I.

Figures 5 and 6 shows the profiles of Θ, Φ, and n_y component of the director for the case of Form B. Like Form A, the defect center also moves to the upper plate and it generates spontaneous distortion (see Figs. 3(a) and 5(a)). Moreover, the n_y component is also the same as that of Form A (see Figs. 4 and 6). The difference is that along the contour that we ploted, Φ changes from $-\pi/2$ to $-\pi$ and then to $\pi/2$. The defect structure can be shown in the order space S^2/Z_2 by Fig. 7(b), also representing a mixed disclination. Comparing Form A with Form B, the difference in initial perturbation leads to the difference in n_y. For our presentation in the order space S^2/Z_2, all of n_y components are redefined to be positive, thus the changes of the quadrants about the director $\boldsymbol{n}$ happen.

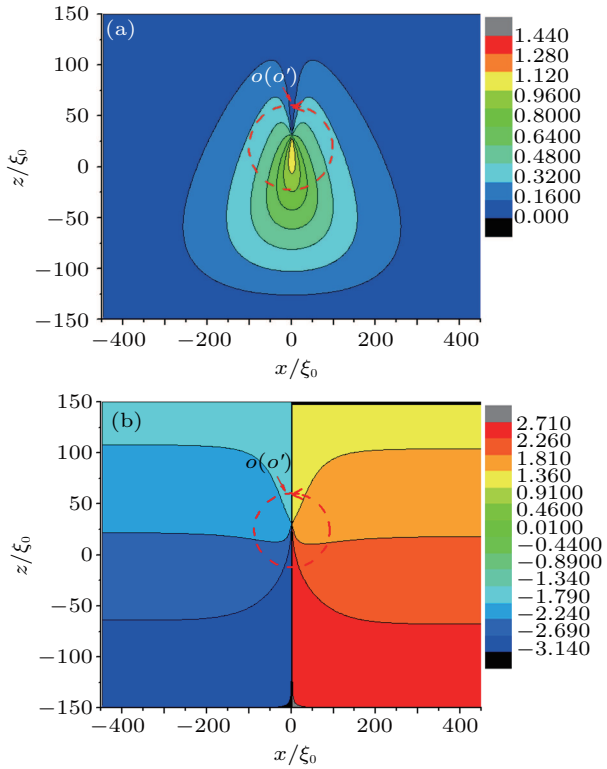


Fig. 5. (color online) Profiles of configurations (a) Θ and (b) Φ of director at equilibrium state for Form B of Model I.

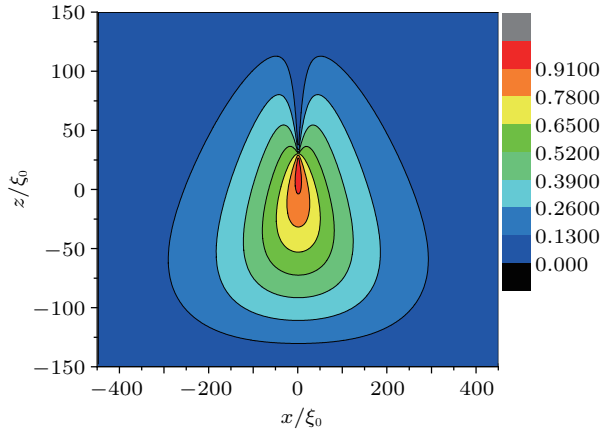


Fig. 6. (color online) Prifile of n_y component of the director at equilibrium state for Form B of Model I.

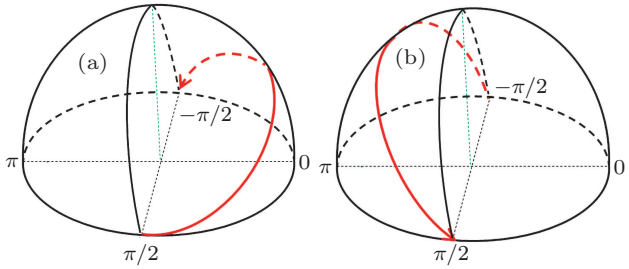


Fig. 7. (color online) Descriptions of mixed defects in the order space S^2/Z_2 for (a) Form A and (b) Form B.

3.1.2. Structures of Forms C and D

In the cases of Forms C and D, the equilibrium states show that the center of the defect moves to the lower plate. Figures 8 and 9 show the profiles of Θ, Φ, and n_y component of the director at equilibrium state for the case of Form C. It is also shown that the elastic anisotropy induces the spontaneous distortion, and the maximum distortion exists near the defect center (see Figs. 8(a) and 9). Along the contour that we plotted, Θ changes from 0 to a maximum value $\Theta_{\max}$ between 0 and $\pi/2$, and then turns back to 0; meanwhile, Φ changes from π to $\pi/2$ and then to 0. The structure can be explained in the order space S^2/Z_2 by Fig. 10(a). Form D generates a similar defect structure to Form C with Φ changing from 0 to $-\pi/2$ and then to $-\pi$, which can be shown in the order space S^2/Z_2 by Fig. 10(b). Figure 10 shows other two mixed disclinations. We need to note here that the starting point o and terminal

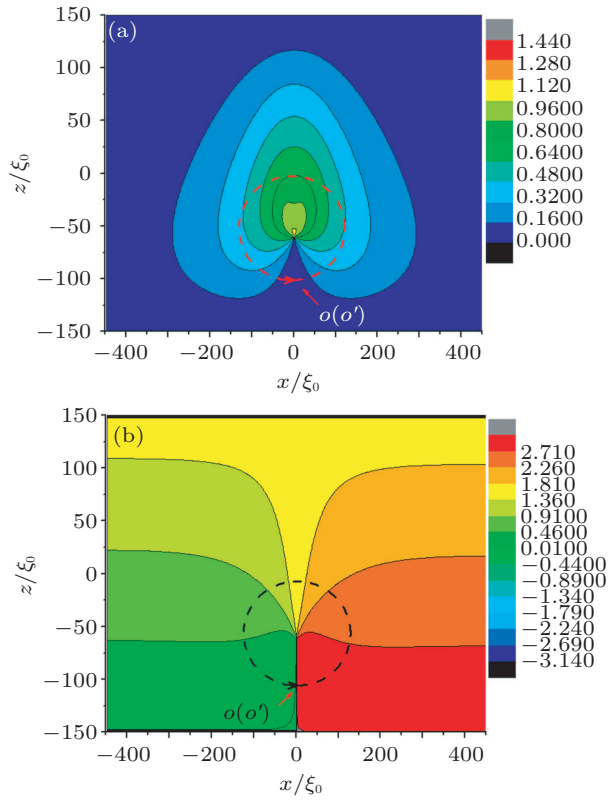


Fig. 8. (color online) Profiles of configurations of (a) Θ and (b) Φ of the director at equilibrium state for Form C of Model I.

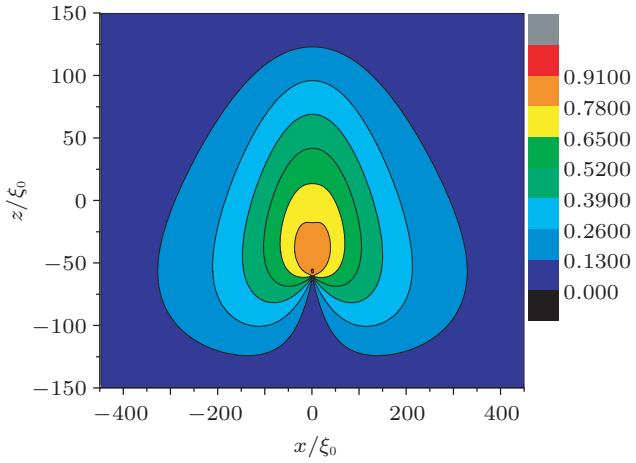


Fig. 9. (color online) Profile of n_y component of the director at equilibrium state for Form C of Model I.

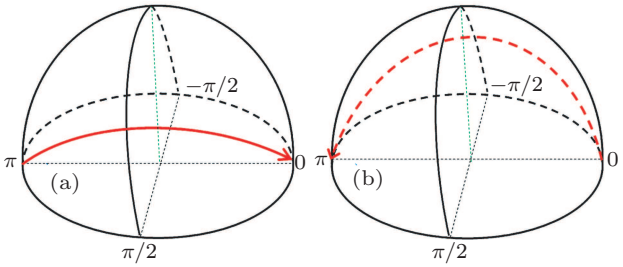


Fig. 10. (color online) Descriptions of mixed defects in the order space S^2/Z_2 for (a) Form C and (b) Form D.

point o' for Forms C and D are different from those of Forms A and B. This is because o and o' are actually the same point, represented by two diametrically opposite points on the bottom circle of the hemisphere, thus we need to choose the points with $\Theta = 0$ as the starting and terminal point.

We make an energy comparison among the four mixed defect structures, where the energy is calculated from our numerical results. The results show that the four new defect structures are quadruple energetically degenerated states.

3.2. Structure transition of Model II

For Model II, four forms of initial twist angles give four similar mixed defect structures to those for Model I, respectively. The defect centers of Forms A and B move upward, while those of Forms C and D move downward. The only difference is the rotation direction of the director $\boldsymbol{n}$. Figure 11 describes the four structures in the order space S^2/Z_2. Compared with Figs. 7 and 10, the opposite rotation directions of the director for Model I and Model II are clearly seen, resulting from the opposite rotation directions of initial $\boldsymbol{n}$.

The energy calculation shows that the four mixed structures are also quadruple energetically degenerated states. Further, the energies of Model I and Model II are identical, indicating the consistency of $M = \pm 1/2$ defects, and they will appear with the same probability.

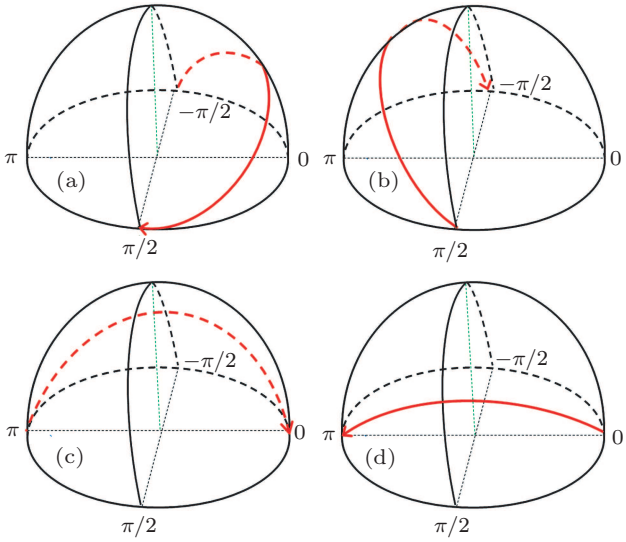


Fig. 11. (color online) Descriptions of mixed defects for (a) Form A, (b) Form B, (c) Form C, and (d) Form D in the order space S^2/Z_2 for Model II.

For comparison, a normal HAN cell without defect is also simulated with the same parameters. For this cell, the elastic anisotropy will not induce the spontaneous distortion, and the structure remains unchanged for different values of L_2/L_1. That is, $n_y \equiv 0$ and $\Theta \equiv 0$ in the normal HAN system. Considering the initial defect structures in Models I and II, we can easily obtain that the joint action of elastic anisotropy and defect biaxiality induces the twist distortion as well as the mixed defect structures. The inexistence of biaxiality in normal HAN leads to no twist distortion.

4. Conclusions

Within Landau-de Gennes theory, we have investigated the spontaneous distortion in HAN cells with $M = \pm 1/2$ defects, using the 2D finite-difference iterative method. Two models are studied, with an $M = -1/2$ wedge defect and $M = +1/2$ wedge defect, respectively. A normal HAN structure with no defect is utilized for conducting comparative studies.

The joint action of elastic anisotropy and defect biaxiality induces spontaneous distortion phenomenon, accompanied by the movement of the defect center to upper or lower plate. Four mixed defect structures appear with the same energy, which we called quadruple energetically degenerated states. The new defect structures do not confine the director $\boldsymbol{n}$ in a 2D plane. It can be deduced that the movement of the defect center will increase with increasing L_2/L_1. A pure HAN system has no twist distortion under the individual effect of elastic anisotropy.

According to the parameters given, we can easily obtain the characteristic length $\xi_o \sim 2.64$ nm, which gives the cell gap $d \sim 0.8$ μm. Maybe the transition structure will change under nano-scale cells. It is our future task to acquire the detailed results. We expect that the main findings of the present

work would appear in other theoretical models, and will provide theoretical guidance for the experimental investigation of the core structures.

References

[1] Mermin N D 1979 *Rev. Mod. Phys.* **51** 591
[2] Trebin H R 1982 *Adv. Phys.* **31** 195
[3] Chaikin P M and Lubensky T C 1995 *Principles of Condensed Matter Physics* (Cambridge: Cambridge University Press)
[4] Meyer R B 1973 *Philos. Mag.* **27** 405
[5] Kléman M and Lavrentovich O D 2003 *Soft Matter Physics* (New York: Springer-verlag)
[6] Fukuda J I 2010 *Phys. Rev. E* **81** 040701
[7] Kurik M V and Lavrentovich O D 1988 *Sov. Phys. Usp.* **31** 196
[8] Kléman M 1983 *Points, Lines and Walls in: Liquid Crystals, Magnetic Systems and Various Disordered Media* (New York: Wiley)
[9] Garel A T 1978 *J. Phys.* **39** 225
[10] Mineev V P 1980 *Sov. Sci. Rev.* **A2** 173
[11] Mori H and Nakanishi H 1988 *J. Phys. Soc. Jpn.* **57** 1281
[12] Nakanishi H, Hayashi K and Mori H 1988 *Commun. Math. Phys.* **117** 203
[13] Zhang C, Grubb A M, Seed A J, Sampson P, Jákli1 A and Lavrentovich O D 2015 *Phys. Rev. Lett.* **115** 087801
[14] Wang X G, Kim Y K, Bukusoglu E, Zhang B, Miller D S and Abbott N L 2016 *Phys. Rev. Lett.* **116** 147801
[15] Schopohl N and Sluckin T J 1987 *Phys. Rev. Lett.* **59** 2582
[16] Bisi F, Gartland E C, Rosso R and Virga E G 2003 *Phys. Rev. E* **68** 021707
[17] Ambrožič M, Kralj S and Virga E G 2007 *Phys. Rev. E* **75** 031708
[18] Zhou S, Shiyanovskii S V, Park H S and Lavrentovich O D 2017 *Nat. Commun.* **8** 14974
[19] De Gennes P G and Prost J 1993 *The Physics of Liquid Crystals* (UK: Oxford University Press)
[20] Virga E G 1994 *Variational Theories for Liquid Crystals* (UK: Chapman Hall)
[21] Kaiser P, Wiese W and Hess S 2015 *J. Non-Equil. Thermody.* **17** 153
[22] Guzmán O, Abbott N L and de Pablo J J 2005 *J. Chem. Phys.* **122** 184711
[23] Zhou X and Zhang Z D 2013 *Int. J. Mol. Sci.* **14** 24135
[24] Zhou X and Zhang Z D 2014 *Liq. Cryst.* **41** 1219
[25] Zhou X, Zhang Z D, Zhang Q and Ye W J 2015 *Materials* **8** 8072
[26] Qian T Z and Sheng P 1997 *Phys. Rev. E* **55** 7111